Materials Chemistry and Physics 132 (2012) 138–144

Contents lists available at SciVerse ScienceDirect

Materials Chemistry and Physics

journal homepage: www.elsevier.com/locate/matchemphys

Structural, electrical and magnetic properties of cadmium substituted nickel–copper ferrites

P.B. Belavi[a], G.N. Chavan[a], L.R. Naik[a,*], R. Somashekar[b], R.K. Kotnala[c]

[a] Department of Studies in Physics, Karnatak University, Dharwad 580 003, India
[b] Department of Studies in Physics, Mysore University, Mysore 570 006, India
[c] National Physical Laboratory, New Delhi 110 012, India

ARTICLE INFO

Article history:
Received 17 March 2011
Received in revised form 31 October 2011
Accepted 11 November 2011

Keywords:
C. FTIR
XRD
SEM
Dc resistivity
Dielectric constant
Saturation magnetization

ABSTRACT

Polycrystalline ferrites with the general formula $Ni_{0.95-x}Cd_xCu_{0.05}Fe_2O_4$ in which x varies from 0.1 to 0.3 were synthesized by standard double sintering ceramic technique. The existence of single phase cubic spinel structure of ferrites was confirmed from XRD measurement. Surface morphology and compositional features were studied by SEM and EDX measurements. Absorption bands observed in FTIR spectra at 600 cm^{-1} (υ_1) and 410 cm^{-1} (υ_2) corresponds to vibrations of tetrahedral and octahedral complexes respectively. In the dc conductivity measurements the decrease of dc resistivity with increase of temperature indicates the semiconducting nature of ferrites. The dielectric measurement of the samples at room temperature studied in the frequency range 20 Hz to 1 MHz shows dispersion in the low frequency region and remains constant at high frequency region. However, the small polaron hoping type of conduction mechanism was inferred from the linear increase of ac conductivity. The magnetic properties of ferrites such as saturation magnetization, magnetic moment and Y–K angles was estimated as a function of cadmium content by VSM technique. The smaller value of Mr/Ms reveals the existence of multidomain (MD) particles in the ferrite samples.

1. Introduction

Polycrystalline ferrites attracted special attention in the field of electronic technology due to their wide applications ranging from microwave to radio wave frequencies. The wide applications of ferrites in various fields created an interest to study the electric and magnetic properties such as high saturation magnetization, stability, resistivity and low loss energy over a wide range of frequency [1–3]. The substituted nickel ferrites are the subject of extensive investigation because of their microwave applications such as circulators, isolators, phase shifters, etc., due to its low electrical conductivity, squareness of hysteresis loop [4,5].

The nickel–copper ferrite has potential application in nanoscience and technology. Cadmium the nonmagnetic divalent metal ion doped with nickel–copper ferrite is of interest in fundamental and applied research. An understanding of their properties as well as variety of applications such as transformers cores, antennas rods and in high quality filters is of special interest [6]. Polycrystalline ferrites have very good dielectric properties; it depends on method of preparation, type of additives and sintering conditions. The electrical conductivity of spinel ferrites is of prime importance as it gives valuable information about the conduction mechanism [7]. The magnetic properties of spinel ferrites strongly depends on the choice of cations along with Fe^{2+} and Fe^{3+} ions and their distribution between tetrahedral (A-site) and octahedral (B-site) sites of the spinel lattice [8]. According to the earlier reports cadmium ions occupy tetrahedral A-site and the substitution of nonmagnetic Cd^{2+} ion in ferrite enhances the magnetic properties like saturation magnetization, magnetic moment [9–12]. The lattice parameter increases due to the increase of cadmium content in the ferrites because of its higher ionic radius compared to other ions in the ferrites. Several researchers have studied the structural, electrical and magnetic properties of substituted ferrites like Ni–Co–Cu [1], Ni–Cd–Zn [12], Ni–Cd [11,13–15], Ni–Cu [16], Mg–Cd [17] and Ni–Mn–Mg [18] mixed ferrites by different methods. However, the literature survey on Ni–Cd–Cu ferrites indicates that not much work has been done on these ferrites. In the present work standard double sintering ceramic technique was used to synthesize the polycrystalline ferrite having the composition $Ni_{0.95-x}Cd_xCu_{0.05}Fe_2O_4$. This method is easier and fabrication of the materials is cheaper as compared to other methods in addition, the grain size and sintering temperatures are easily controllable. The present work is focused on the study of structural, electric

* Corresponding author. Tel.: +91 0836 2215316; fax: +91 836 2747884.
E-mail addresses: naik_36@rediffmail.com, lalasingn@gmail.com (L.R. Naik).

0254-0584/$ – see front matter © 2011 Elsevier B.V. All rights reserved.
doi:10.1016/j.matchemphys.2011.11.009

and magnetic properties of cadmium substituted nickel–copper ferrites.

2. Experimental details

2.1. Synthesis

Polycrystalline ferrite system $Ni_{0.95-x}Cd_xCu_{0.05}Fe_2O_4$ with composition $x = 0.1$, 0.2 and 0.3 were synthesized by standard double sintering ceramic technique. The samples were prepared by thoroughly mixing AR grade NiO, CdO, CuO and Fe_2O_3 oxides in stoichiometric ratio and later on well grounded in a planetary agate mortar for few hours. The powder samples were presintered at 800 °C for 8 h in a programmable furnace and slowly cooled to room temperature. The sintered powders were mixed with 2% of PVA as a binder and uniaxially pressed at a pressure of about 7 tons cm^{-2} to form pellets of 10 mm diameter and 2–3 mm thickness. These pellets were finally sintered at 1150 °C for 12 h in a programmable furnace to remove the organic binder.

2.2. Characterization

The powder samples of ferrites were characterized by using X-ray diffractometer (Philips model PW-1710) with Cu-Kα radiation (λ = 1.5405 Å) and the lattice parameter of the synthesized samples were estimated using the relation [13]

$$a = d_{hkl}\sqrt{(h^2 + k^2 + l^2)} \tag{1}$$

The X-ray densities of the samples were estimated using the relation [15]

$$dx = \frac{ZM}{Na^3} \tag{2}$$

where Z is the number of molecules per unit cell of spinel lattice, M is the molecular weight of the samples, N is the Avogadro's number and a is the lattice parameter of the samples.

The porosity of the sample was estimated using the formula

$$p = 1 - \frac{da}{dx} \times 100\% \tag{3}$$

where da is actual density and dx is X-ray density of the sample.

The average crystallite size and strain induced inside the samples has been estimated using the Williamson-Hall plot relation [19].

$$\beta \cos\,\theta = \frac{k\lambda}{D} + 4\varepsilon \sin\theta \tag{4}$$

where D is the average crystallite size, k is a constant, λ is the wavelength, β is the full width half maximum of diffraction peaks, ε is the strain induced inside the samples and θ the Bragg's angle.

The surface morphology and compositional features were studied using scanning electron microscopy (SEM) and energy dispersive X-ray spectroscopy (EDX) techniques (ESEM Quanta 200, FEI). IR studies were carried out by FTIR spectrometer (Nicolet, model-*Impact*, 410, USA) from 400 cm^{-1} to 800 cm^{-1} to assign the vibrations of ferrites (tetrahedral/octahedral).

Electrical conductivity (dc) of the samples was studied after silver pasting the two polished surfaces of each pellet. The temperature dependent dc resistivity were carried out by using two probe method and was estimated by using the following relation

$$\rho = \frac{R\pi r^2}{t} \tag{5}$$

where R is the resistance, r is the radius; t is the thickness of the samples.

The drift mobility of the samples were estimated using the relation

$$\mu_d = \frac{1}{ne\rho} \tag{6}$$

where e is the charge of electron, ρ is the resistivity, n is the charge carrier concentration and which is calculated using the following relation [14]

$$n = \frac{N\rho_m P_{Fe}}{M} \tag{7}$$

where ρ_m is the measured density, P_{Fe} is the number of iron atoms in the ferrites.

The dielectric measurements were carried out in the frequency range 20 Hz to 1 MHz at room temperature using an impedance analyzer (Model 6540A Wayne Kerr, UK).

The ac conductivity of the ferrites was calculated using the relation

$$\sigma_{ac} = \varepsilon'\varepsilon_o\omega \tan\delta \tag{8}$$

where ε' is the dielectric constant, ε_o is the permittivity of free space, ω is the angular frequency, $\tan\delta$ is the loss tangent.

Vibrating sample magnetometer (VSM model 735 LakeShore) was used to measure the saturation magnetization and magnetic moment (in Bohr magneton) and can be estimated by using the following relation [6]

$$\mu_B = \frac{M\sigma'_s}{5585} \tag{9}$$

where M is the molecular weight of the samples, σ'_s is the magnetization per gram of the samples.

The Y–K angles of ferrite samples were estimated using the following relation [13]

$$\cos\,\alpha_{yk} = \frac{n_B + 5(1-x)}{7(1+x)} \tag{10}$$

where n_B is the Bohr magneton, x is the concentration of substituted ion.

3. Results and discussion

3.1. X-ray diffraction

The X-ray diffraction pattern of ferrite samples is shown in Fig. 1. And all the peaks appeared in the diffraction patterns are identified with the help of JCPD'S data and confirmed the formation of cubic spinel structure of single phase ferrite without impurities. The lattice parameters of the ferrite samples were estimated using the relation (1) for the prominent peak (3 1 1) and listed in Table 1. The lattice parameter, X-ray density and porosity increases with increase of Cd^{2+} content in the ferrite systems. This is because the Cd^{2+} ion have larger ionic radii (0.097 nm) than that of Cu^{2+} (0.073 nm), Ni^{2+} (0.069 nm) and Fe^{3+} (0.0645 nm) ions [20]. The average crystallite size and strain induced inside the ferrite sample was estimated from the intercept and slope of the Williamson-Hall plot shown in Fig. 2 (for $x = 0.1$) and it is to be noted that as the cadmium content increases strain induced inside the sample increases (Table 1).

3.2. Scanning electron microscopy

The SEM micrographs of ferrite samples are shown in Fig. 3(a–c). These figures show fine particles in all the samples without segregation of impurity. The average grain size estimated by Cottrell's method [21] lies in the range of 1.256–1.759 μm. The average grain size increases with decreasing the grain boundary area, as this grain

Table 1
Lattice parameter (a), X-ray density (dx), porosity (p), average crystalline size (D), strain (ε), tetrahedral (k_t) and octahedral (k_o) force constant.

(x)	a (Å)	dx (g cm^{-3})	p (%)	D (nm)	ε (%), $\times 10^{-3}$	Force constants (N m^{-1})	
						$k_t \times 10^2$	$k_o \times 10^2$
0.1	8.364	5.45	14.49	94.33	1.94	1.698	1.183
0.2	8.402	5.49	13.11	141.75	3.17	1.830	1.177
0.3	8.424	5.58	12.90	149.68	3.63	1.949	1.164

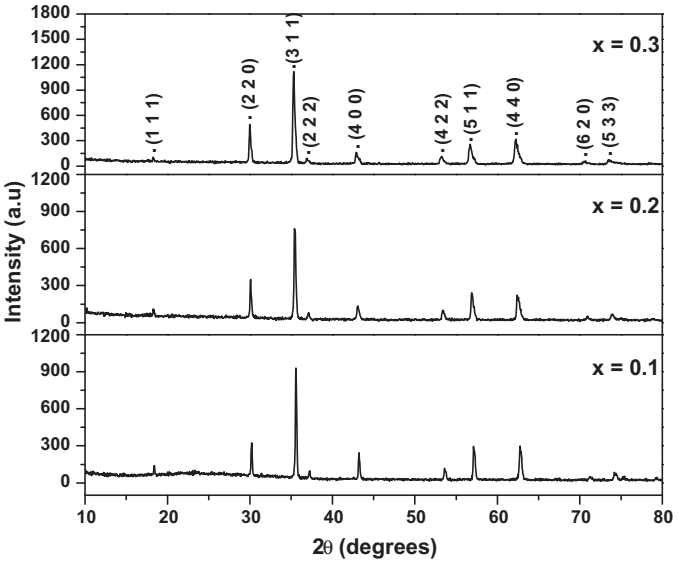

Fig. 1. XRD patterns of $Ni_{0.95-x}Cd_xCu_{0.05}Fe_2O_4$ (x = 0.1, 0.2, 0.3) ferrites.

boundary area acts as an obstacle for domain wall motion. The presence of pores in the sample breaks the magnetic circuit between the grains and thus the net magnetization decreases due to the increase of porosity and vice versa. In the present ferrite samples the net magnetization increases due to the decrease of porosity. The chemical compositions of the present ferrite samples after final sintering were determined by energy dispersive X-ray spectroscopy (EDX) and which is shown in Fig. 4(a–c). The EDX spectra of the ferrite samples show the presence of elements (Ni, Cd, Cu, Fe and O) without impurities and which indicates the completeness of solid state reaction.

3.3. FTIR studies

Fig. 5 shows FTIR spectra of the ferrite samples in the range of wave numbers from 400 to 800 cm^{-1}. The two absorption bands

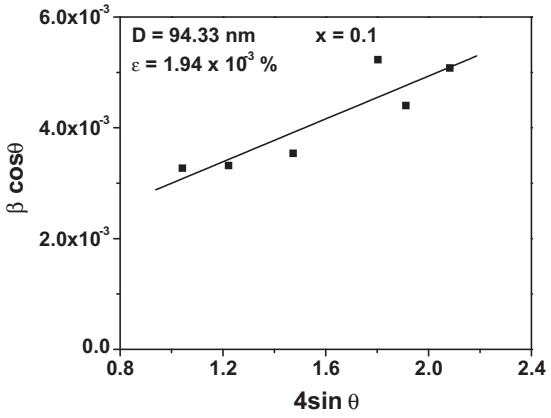

Fig. 2. Williamson-Hall plot of $Ni_{0.95-x}Cd_xCu_{0.05}Fe_2O_4$ ferrites.

observed at 600 cm^{-1} (υ_1) and 410 cm^{-1} (υ_2) corresponds to vibrations of tetrahedral and octahedral complexes respectively, and according to Waldron which confirms the formation of single phase cubic spinel structure of ferrites [22,23]. From the figures it is to be noted that the shifting of band position (600 cm^{-1}) υ_1 towards lower wavelength region is due to the increase of Cd^{2+} ion in ferrite and preferably occupies the (A-site) tetrahedral site [9,10]. However, Ni^{2+} and Cu^{2+} ions occupy the (B-site) octahedral site [24], but Fe^{3+} ions occupy both tetrahedral and octahedral sites. Substitution of Cd^{2+} ion in the system decreases the amount of Ni^{2+} and increases the amount of Fe^{3+} ions in the octahedral B-site and shifts band position at (410 cm^{-1}) υ_2 towards lower wavelength. The cation distribution of ferrites are represented as follows

$$(Cd_xFe_{1-x})^A[Ni_{0.95-x}Cu_{0.05}Fe_{1+x}]^BO_4{}^{2-} \quad (11)$$

The force constant for tetrahedral site (k_t) and octahedral site (k_o) were estimated by employing the method suggested by Waldron [23] and according to them the force constant k_t and k_o are given as follows

$$k_t = 7.62 \times M_1 \times \upsilon_1^2 \times 10^{-7} \text{ N m}^{-1} \quad (12)$$

$$k_o = 10.62 \times \frac{M_2}{2} \times \upsilon_2^2 \times 10^{-7} \text{ N m}^{-1} \quad (13)$$

where M_1 and M_2 are respectively the molecular weights of cations in A- and B-sites.

The estimated values of k_t and k_o are listed in Table 1. The octahedral force constant decreases as cadmium content increases in the ferrite system. The addition of Cd^{2+} ion content in the tetrahedral site (A-site) successively transfers Fe^{3+} ions from tetrahedral to octahedral site (B-site) and which is responsible for the decrease of the octahedral force constant. In other words due to addition of Cd^{2+} ion the charge imbalance in the system takes place and hence the oxygen ions are likely to move away from Fe^{3+} ions which in turn reduce the octahedral force constant [25].

3.4. Dc resistivity

Fig. 6 shows variation of dc resistivity with temperature for all the ferrite samples. The decrease of resistivity with increase of temperature indicates the semiconducting nature of ferrites. The conduction mechanism in ferrites was explained on the basis of Verwey and De Boer [26] mechanism, which involves the exchange of electrons between the ions of the same elements present in more than one valence state and randomly distributed over crystallographic equivalent lattice cites. The exchange of electrons between $Fe^{2+} \leftrightarrow Fe^{3+} + e^-$ is responsible for n-type charge carrier and the exchange of holes between $Ni^{3+} \leftrightarrow Ni^{2+} + e^+$, $Cu^{2+} \leftrightarrow Cu^{1+} + e^+$ and $Cd^{2+} \leftrightarrow Cd^{1+} + e^+$ are responsible for p-type charge carriers in the ferrite phase. The number of such ions depends upon the sintering condition and amount of reduction of Fe^{2+} to Fe^{3+} ions at elevated firing temperature. The change in slope is observed in all the ferrite samples and such a change in slope is either due to Curie temperature or due to the change in conduction mechanism [27]. Arrhenius

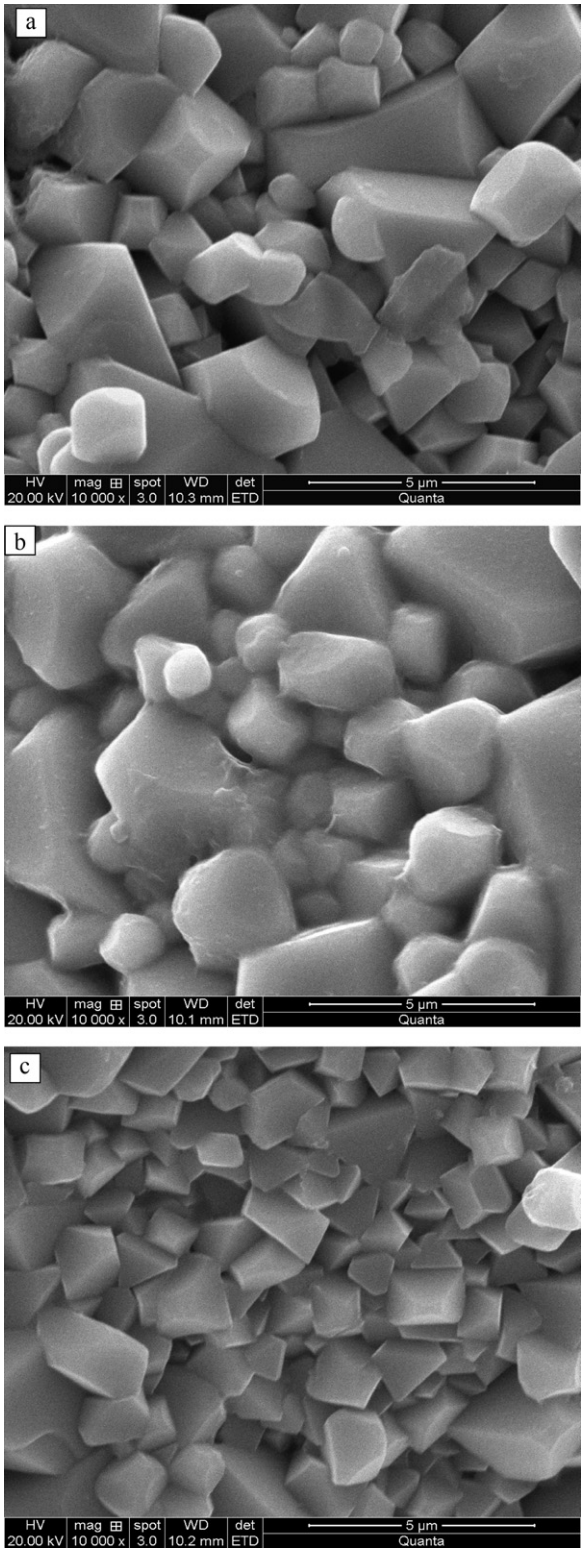

Fig. 3. SEM micrographs of $Ni_{0.95-x}Cd_xCu_{0.05}Fe_2O_4$ ferrites with (a) $x = 0.1$, (b) $x = 0.2$, (c) $x = 0.3$.

relation for the decrease in resistivity with increase in the temperature [28] is given as

$$\rho = \rho_o \exp\left(\frac{\Delta E}{K_B T}\right) \quad (14)$$

where ΔE is the activation energy, it is the energy required to release an electron from one ion to the neighboring due to an

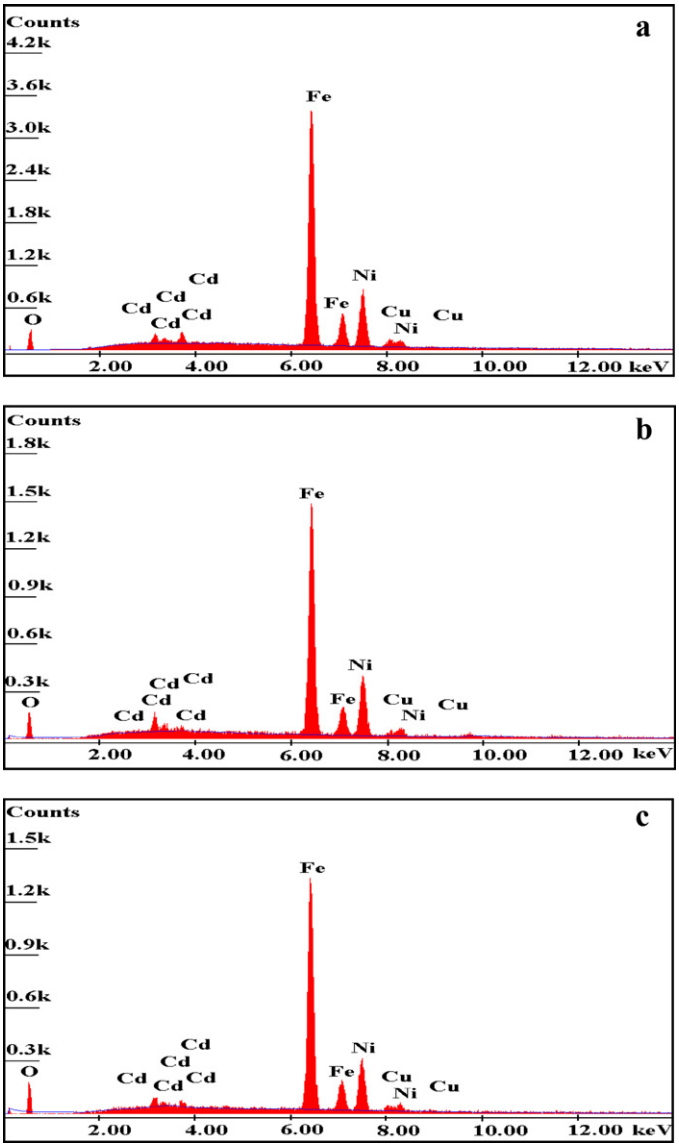

Fig. 4. EDX spectra of $Ni_{0.95-x}Cd_xCu_{0.05}Fe_2O_4$ ferrites with, (a) $x = 0.1$, (b) $x = 0.2$, (c) $x = 0.3$.

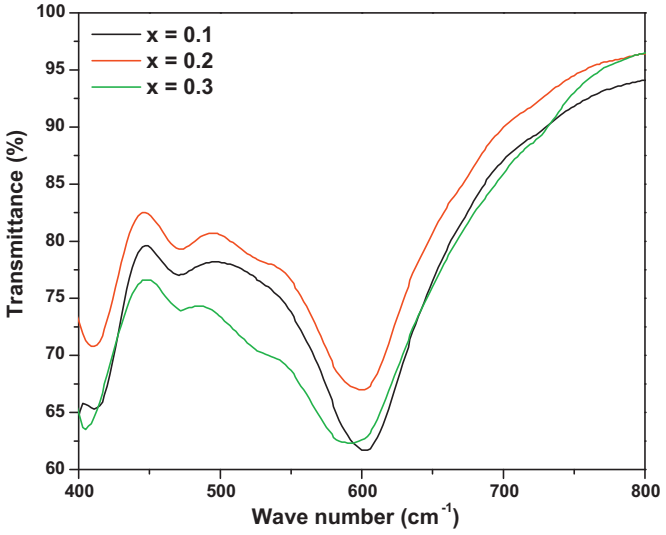

Fig. 5. FTIR transmission spectra of $Ni_{0.95-x}Cd_xCu_{0.05}Fe_2O_4$ ($x = 0.1, 0.2, 0.3$) ferrites.

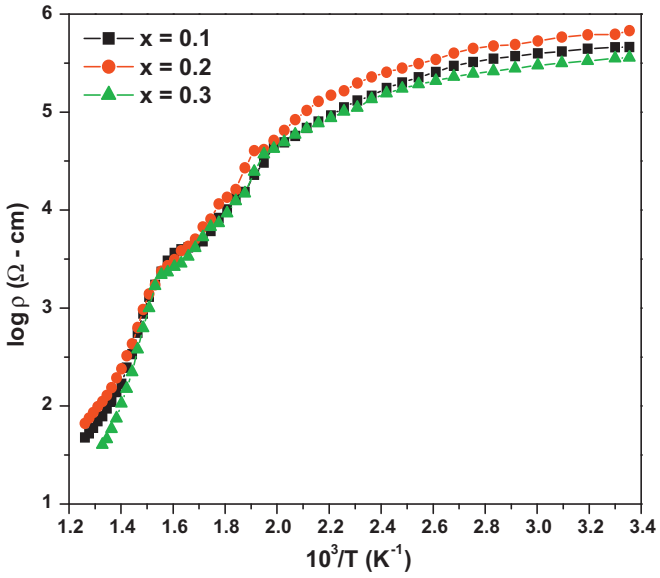

Fig. 6. Variation of dc resistivity with temperature of $Ni_{0.95-x}Cd_xCu_{0.05}Fe_2O_4$ ($x = 0.1$, 0.2, 0.3) ferrites.

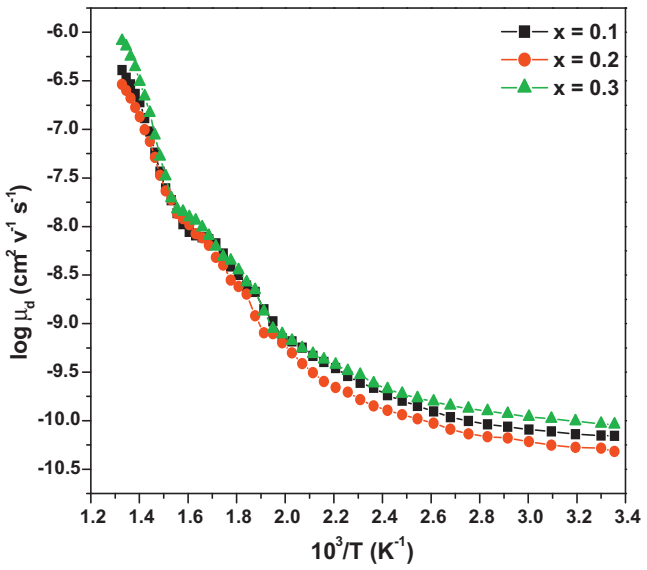

Fig. 7. Variation of drift mobility with temperature of $Ni_{0.95-x}Cd_xCu_{0.05}Fe_2O_4$ ($x = 0.1$, 0.2, 0.3) ferrites.

electrical conductivity, K_B is the Boltzmann constant and T is the absolute temperature. For all the ferrite samples the break near the Curie temperature is due to the transition from ferromagnetic to paramagnetic region. The activation energy of paramagnetic (ΔE_1) and ferromagnetic (ΔE_2) regions are calculated from the slopes of paramagnetic and ferromagnetic regions using the following relation [28]

$$\Delta E = 1.98 \times 10^{-4} \times slope \quad (15)$$

The estimated values listed in Table 2 shows greater activation energy in the paramagnetic region than in the ferromagnetic region and are in good agreement with the theory of Irkin and Turor [29]. The lowering of activation energy in the ferromagnetic region is attributed to the spin disordering effect [30]. However, the activation energy observed for all the ferrite samples (>0.2 eV) indicates the small polaron hopping type of conduction mechanism in ferrites.

According to small polaron hopping type of conduction mechanism the decrease of resistivity as a function of temperature is due to the increase in thermally activated drift mobility of charge carriers. The plot of drift mobility as a function of temperature (Fig. 7) shows increase of drift mobility with increasing temperature for all the samples. Charge carriers overcome the activation energy barrier resulting increase in their mobility by getting additional energy due to the increase of temperature.

3.5. Dielectric properties

Fig. 8 shows the variations of dielectric constant with frequency. The dielectric constant decreases with increase in frequency and a rapid decrease in the low frequency region (20 Hz to 1 kHz) attains saturation at high frequency region (1 kHz to 1 MHz). The rapid decrease of dielectric constant in the low frequency region (20 Hz to 1 kHz) shows usual dielectric dispersion. This variation can be explained on the basis of space charge polarization model of Maxwell–Wagner [31,32] type of interfacial polarization in accordance with koops phenomenological theory [33]. The dielectric dispersion is more for the sample with $x = 0.1$ and it is due to the availability of large number of ferrous ions on A-site of the system.

The larger value of dielectric constant at lower frequency is due to the predominance of Fe^{2+} ions, interfacial dislocation pile ups, oxygen vacancies, grain boundaries, defects, etc. The maximum values of dielectric constants are due to availability of space charge polarization at the grain boundaries [34]. The electron exchange between the ferrous and ferric ions, i.e. $Fe^{2+} \leftrightarrow Fe^{3+}$ at the grain boundary region is responsible for polarization which inturn increases the dielectric constant. However, the polarization decreases with increase in frequency and then reaches a constant value but beyond the externally applied electric field of frequency 1 kHz the electron exchange between $Fe^{2+} \leftrightarrow Fe^{3+}$ cannot follow the alternating field [35].

The variations of dielectric loss tangent with frequency for the samples are shown in Fig. 9. It shows dielectric dispersion at lower frequency region and a peak at higher frequency region, it may be due to the existence of resonance between applied frequency and hopping frequency of charge carriers [36] and also due to the domain wall resonance (i.e. grain–grain boundary contribution) [37].

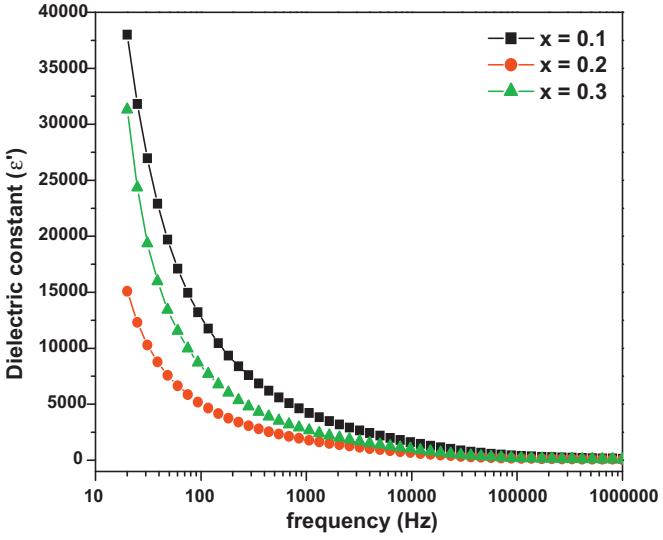

Fig. 8. Frequency dependent variation of dielectric constant of $Ni_{0.95-x}Cd_xCu_{0.05}Fe_2O_4$ ($x = 0.1$, 0.2, 0.3) ferrites.

Table 2
Activation energy (ΔE) saturation magnetization (Ms), magnetic moment (μ_B), ratio of Mr/Ms and Y–K angles (α_{yk}).

(x)	Activation energy (eV)		Ms (emu g^{-1})	μ_B	Mr/Ms	α_{yk} (/°C)
	ΔE_1	ΔE_2				
0.1	1.032	0.520	35.547	0.327	0.036	51.17
0.2	1.233	0.573	59.307	0.546	0.029	57.23
0.3	1.272	0.609	63.847	0.589	0.022	63.29

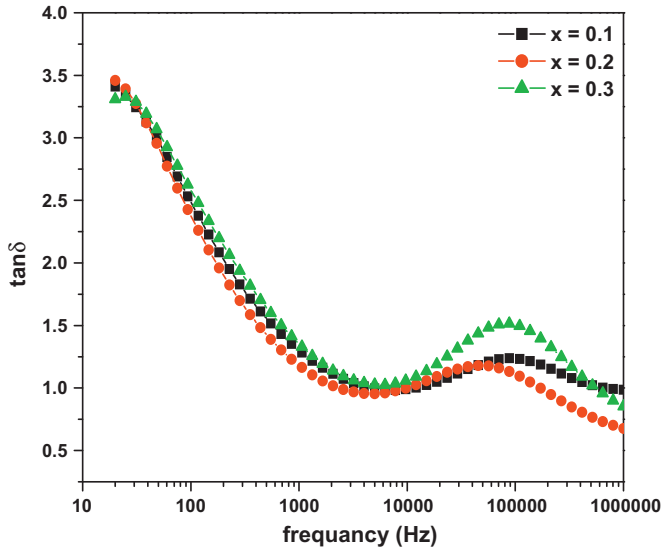

Fig. 9. Frequency dependent variation of dielectric loss of $Ni_{0.95-x}Cd_xCu_{0.05}Fe_2O_4$ (x = 0.1, 0.2, 0.3) ferrites.

Fig. 10 shows the variation of ac conductivity with frequency for the ferrite samples. The plot shows linear increase of ac conductivity with increasing frequency that is ac conductivity in disordered solids is directly proportional to frequency. The linear increase of conductivity with frequency was due to small polaron hopping type of conduction mechanism and decrease of conductivity with increase of frequency was due to the large polaron hopping type of conduction mechanism in ferrites [38]. However a slight decrease in conductivity at certain frequency is attributed to mixed polarons (i.e. small and large).

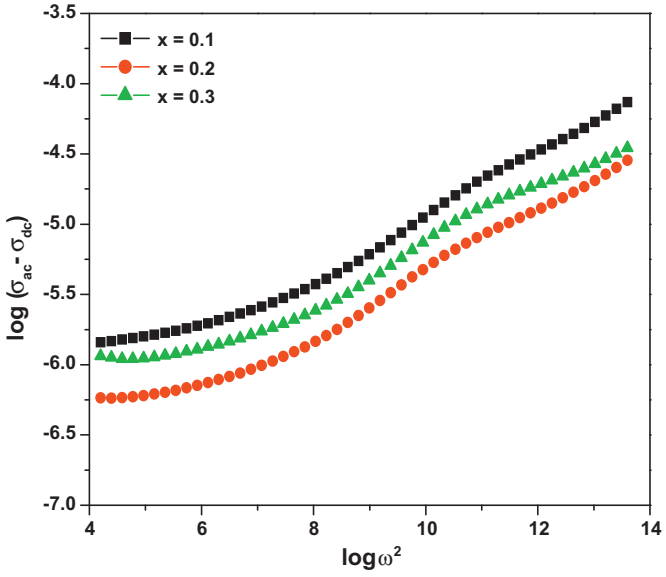

Fig. 10. Variation of ac conductivity with frequency of $Ni_{0.95-x}Cd_xCu_{0.05}Fe_2O_4$ (x = 0.1, 0.2, 0.3) ferrites.

3.6. Magnetic hysteresis studies

Fig. 11 shows the magnetic hysteresis loops of ferrite samples. The hysteresis loops of all ferrite samples shifts towards field axis with decrease of the cadmium content in the ferrites. The estimated values of saturation magnetization, magnetic moment, Mr/Ms and Y–K angles for the ferrite samples are listed in Table 2. The increase of saturation magnetization, magnetic moment and Y–K angles with increase of the cadmium content was attributed to the surface spin effect and cation distribution on A-site and B-site. The Cd^{2+} ion strongly occupies the tetrahedral A-site [9,10], while Ni^{2+} and Cu^{2+} ions occupies the octahedral B-site [24] and Fe^{3+} ions occupies both tetrahedral and octahedral site. The addition of cadmium a non-magnetic divalent metal ion (Cd^{2+} ion) content in ferrites reduces the amount of Ni^{2+} ions and increases the amount of Fe^{3+} ions in ferrites on B-site was responsible for the increase of saturation magnetization and magnetic moment, obeys Nell's two sub lattice model and it suggests the existence of canted spins giving rise to Y–K angles [39].

The occupancy of Cd^{2+} ion at tetrahedral site (A-site) successively replace Fe^{3+} ions from A-site and transfers equal amount of Fe^{3+} ions to B-site. The decrease of magnetic moment of tetrahedral site with increase of Cd^{2+} ion content is due to the decrease of Fe^{3+} ions content on A-site. The addition of Cd^{2+} ion in the ferrites decreases the amount of Ni^{2+} ion and increases the amount of Fe^{3+} ions on B-site, increases the magnetic moment of octahedral site (B-site). And the increase of net magnetic moment (μ_B) in the ferrites was suggested to the Yafet–Kittel (Y–K) spin arrangement.

The estimated Y–K angles are found to increase with increasing Cd^{2+} ion content (Table 2). The variation of saturation magnetization and magnetic moment with Cd^{2+} ion content can also be

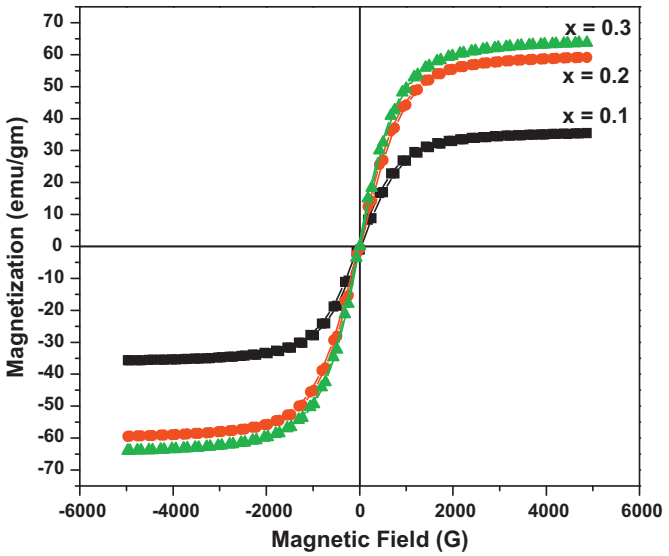

Fig. 11. VSM analysis of $Ni_{0.95-x}Cd_xCu_{0.05}Fe_2O_4$ (x = 0.1, 0.2, 0.3) ferrites.

explained on the basis of Nell's two sub lattice model. According to this model three types of exchange interactions are possible (i.e., A–A, B–B and A–B). Out of the three interactions A–B interaction is strong and effective. The strength of A–B interaction increases with the occupancy of Cd^{2+} ion in A-site with successive transfers of Fe^{3+} ions to B-site and is responsible for the increase of saturation magnetization and magnetic moment. However, the small values of Mr/Ms are due to the existence of multidomain (MD) particles in all the samples [28].

4. Conclusions

Polycrystalline ferrites with composition $Ni_{0.95-x}Cd_xCu_{0.05}Fe_2O_4$ have been successfully synthesized by standard double sintering ceramic technique. The X-ray diffraction pattern reveals the confirmation of single phase cubic spinel structure of all the ferrites. The lattice parameter increases with increasing the cadmium content in ferrites. The SEM micrograph of all the samples shows fine particles without segregation of impurity. The presence of Ni, Cd, Cu, Fe and O elements in the ferrite samples were confirmed from EDX measurements. The decrease of dc resistivity with increase of temperature for all the samples indicates the semiconducting nature of ferrites. The variation of dielectric constant with frequency shows the usual dielectric dispersion in the low frequency region and almost remains constant in the high frequency region. The linear increase of ac conductivity with frequency suggests small polarons hopping type of conduction mechanism in ferrites. Saturation magnetization, magnetic moment and Y–K angles are found to increase with cadmium content. The small values of Mr/Ms suggest the existence of MD particles in all the samples.

Acknowledgements

One of the author (LRN) thanks to UGC, New Delhi, for sanctioning the major research project. The author (PBB) thanks to UGC, New Delhi, for providing a project fellowship in the major research project (F.No.34-34/2008 (SR) dated. 30/12/2008) sanctioned to Dr. L.R. Naik. Thanks to Dr. Jyoti. Shah, NPL, New Delhi, for the technical help.

References

[1] R.S. Devan, Y.D. Kolekar, B.K. Chougule, J. Phys.: Condens. Matter 18 (2006) 9809.
[2] A.M. Abdeen, J. Magn. Magn. Mater. 185 (1998) 199.
[3] S.S. Bellad, S.C. Watwe, B.K. Chougule, Mater. Res. Bull. 37 (7) (1999) 1099.
[4] A.S. Waingankar, S.G. Kulkarni, M.S. Sagare, J. Phys. IV (1997) 155.
[5] O.H. Kwon, Y. Fukushima, M. Sugimoto, N. Hiratsuka, J. Phys. IV (1997) 165.
[6] P.P. Hankare, M.R. Kadam, R.P. Patil, K.M. Garadkar, R. Sasikala, A.K. Tripathi, J. Alloys Compd. 501 (2010) 37.
[7] J.M. Song, J.G. Koh, J. Magn. Magn. Mater. 152 (1996) 383.
[8] M.K. Shobana, S. Sankar, J. Magn. Magn. Mater. 321 (2009) 3132.
[9] S.A. Patil, V.C. Mahajan, A.K. Gatge, S.D. Lotake, Mater. Chem. Phys. 57 (1998) 86.
[10] O.M. Hemeda, M.M. Barakat, J. Magn. Magn. Mater. 223 (2001) 127.
[11] S.P. Jadhav, B.G. Toksha, K.M. Jadhav, N.D. Shinde, Chin. J. Chem. Phys. 23 (4) (2010) 459.
[12] M.S.R. Prasad, B.B.V.S.V. Prasad, B. Rajesh, K.H. Rao, K.V. Ramesh, J. Magn. Magn. Mater. 323 (2011) 2115.
[13] A.K. Nikumbh, A.V. Nagawade, G.S. Gugale, M.G. Chaskar, P.P. Bakare, J. Mater. Sci. 37 (2002) 637.
[14] M.B. Shelar, P.A. Jadhav, S.S. Chougule, M.M. Mallapur, B.K. Chougule, J. Alloys Compd. 476 (2009) 760.
[15] K.B. Modi, M.K. Rangolia, M.C. Chhantbar, H.H. Joshi, J. Mater. Sci. 41 (2006) 7308.
[16] S.M. Hoque, Md.A. Choudherry, Md.F. Islam, J. Magn. Magn. Mater. 251 (2002) 292.
[17] A.B. Gadkari, T.J. Shinde, P.N. Vasambekar, J. Mater. Sci. Mater. Electron. 21 (2010) 96.
[18] M.A. Ahmed, S.T. Bishay, S.I. El-dek, G. Omar, J. Alloys Compd. 509 (2011) 805.
[19] X.D. Zhou, W. Huebner, Appl. Phys. Lett. 79 (21) (2001) 3512.
[20] http://environmentalchemistry.com/yogi/periodic/.
[21] A. Cottrell, An Introduction to Metallurgy, Edward Arnold Publishing Ltd., London, 1967.
[22] B.P. Ladgaonkar, C.B. Kolekar, A.S. Vaingankar, Bull. Mater. Sci. 25 (4) (2002) 351.
[23] R.D. Waldron, Phys. Rev. 99 (1955) 1727.
[24] G.K. Joshi, A.Y. Khot, S.R. Savant, Solid State Commun. 65 (1988) 1593.
[25] W.D. Kingery, H.K. Bowen, D.R. Uhlmann, Introduction to Ceramics, Wiley, New York, 1975, p. 904.
[26] E.J.W. Verwey, F.De. Boer, J.H. Vsanten, J. Chem. Phys. 161 (1948) 1091.
[27] D. Ravinder, B. Ravikumar, Mater. Lett. 57 (2003) 4471.
[28] B.K. Bammannavar, L.R. Naik, R.B. Pujar, B.K. Chougule, Indian J. Eng. Mater. Sci. 14 (2007) 381.
[29] Y.P. Irkin, E.A. Turor, Sovt. Phys. JEPT 33 (1957) 673.
[30] A. Dais, R.L. Moreira, J. Mater. Res. 12 (1998) 2190.
[31] J.C. Maxwell, Electricity and Magnetism, vol. 2, Oxford University Press, New York, 1973, p. 828.
[32] K.W. Wagner, Am. J. Phys. 40 (1993) 817.
[33] C.G. Koops, Phys. Rev. 83 (1951) 121.
[34] L.T. Rabinkin, Z.I. Novikova, Acad. Nauk. USSR Minsk. (1960) 146.
[35] N. Popandan, P. Balay, A. Narayansamy, J. Phys.: Condens. Matter 14 (2002) 3221.
[36] D. Ravinder, K. Vijayakumar, Bull. Mater. Sci. 24 (5) (2001) 505.
[37] V.L. Mathe, K.K. Patanakar, M.B. Kothale, S.B. Kulakarni, P.B. Joshi, S.A. Patil, Pramana – J. Phys. 58 (5 and 6) (2002) 1105.
[38] D. Alder, J. Feinleib, Phys. Rev. B 2 (1970) 3112.
[39] Y. Yafet, C. Kittel, Phys. Rev. 87 (1952) 290.